Dark plasmon modes for efficient hot electron generation in multilayers of gold nanoparticles.

Dominik Hoeing,[1, 2, a)] Florian Schulz,[1] Niclas S. Mueller,[3] Stephanie Reich,[3] and Holger Lange[1, 2, b)]

[1)]*Institute for Physical Chemistry, Universität Hamburg, Martin-Luther-King Platz 6, 20146 Hamburg, Germany*

[2)]*CUI:Advanced Imaging of Matter, Luruper Chaussee 146, 22761 Hamburg, Germany*

[3)]*Department of Physics, Freie Universität Berlin, Arnimallee 14, 14195 Berlin, Germany*

(Dated: 7 January 2020)

The excitation of dark plasmons, i.e. coupled plasmon modes with a vanishing net dipole, is expected to favor Landau damping over radiative damping. The dark plasmon excitation might therefore lead to an increased absorption of energy within gold nanoparticles, resulting in a strong generation of hot electrons compared to the generation via bright plasmons. We performed transient-absorption spectroscopy on gold nanoparticle films to assess the initial electronic temperature before thermalization. We observe a significant increase in the electron-phonon coupling time if dark plasmon modes are excited in these films. The results indicate an efficient energy absorption within the nanoparticles due to the suppressed radiative decay of dark plasmon modes.

[a)]Electronic mail: Dominik.Hoeing@chemie.uni-hamburg.de

[b)]Electronic mail: Holger.Lange@chemie.uni-hamburg.de

I. INTRODUCTION

The generation of hot charge carriers in plasmonic gold nanoparticles (AuNPs) has seen considerable attention by the research community in recent years, because it not only allows studying fundamental light-matter interactions[1], but is also thought to be useful for a variety of applications like photocatalysis[2,3] or solar cells[4,5]. The main focus of recent studies revolve around building nanoparticle systems that lead to an efficient excitation and long lifetimes of hot carriers. Hot carriers are a product of plasmon damping, which occurs mainly via elastic and inelastic electron-electron scattering, scattering on phonons, and Landau damping.[6,7] Landau damping, which refers to electron scattering at the nanoparticle surface, turns plasmon quanta into excited electron-hole pairs. A competitive process is the radiative plasmon damping via photon scattering. Radiative damping by light scattering reduces the amount of energy stored in the plasmon mode and the amount of energy that is turned into excited carriers via internal damping.[6,8] For example, in disordered layers of 12 nm AuNPs Feldstein et al.[9] observed decreasing electron-phonon coupling times with increasing film thickness, which has been attributed to the competing effects of increased surface scattering and electron oscillation-phonon resonance detuning.[9] In recent studies we have reported how dark plasmon modes, i.e. coupled plasmon modes with a vanishing net dipole moment, can be excited in self-assembled multilayers of hexagonally close-packed AuNPs.[10] These plasmon modes lead to new absorption peaks in the near infrared spectral region with the vanishing net dipole diminishing their radiative decay. A first study of the hot electron dynamics in AuNP assemblies already hinted at an increased absorption within the AuNPs, accompanied by an increased hot electron generation due to dark plasmon excitations, but was inconclusive due to a lack of control of the number of layers[11]. Here, we investigate the relationship between the layer number and the generation of hot electrons due to the decay of dark plasmon modes. We hypothesize that the increase in absorption due to dark plasmon resonances directly leads to an increased generation of hot electrons in AuNP multilayers compared to monolayers, which do not show these types of plasmon modes.

II. THEORY

Plasmon coupling is the result of the dipole-dipole interaction of proximate plasmonic particles.[12,13] Plasmons of two adjacent particles can hybridize such that the plasmonic dipoles align parallel or

antiparallel to each other.[10] Modes with parallel dipoles are referred to as bright plasmon modes as these are excitable by an electromagnetic far field. In contrast, dark plasmon modes occur for an antiparallel orientation of the plasmonic dipoles, as sketched in Fig 1. In the far field, the plasmonic dipoles cancel each other which leads to reduced radiative damping and light scattering. Normally, dark plasmons are not excitable by an external electric field due to this vanishing net dipole. However, we have shown recently that an increased influence of field retardation in combination with the large refractive index of AuNP layers allows exciting dark plasmons in bilayers of hexagonally close-packed AuNP with visible light at normal incidence - given a sufficient particle size of more than approximately 30 nm.[10,14]

As presented in Fig. 1b, for such a AuNP bilayer the excitation of a dark plasmon mode leads to an additional absorbance peak at the edge between the visible and near infrared spectrum. This peak is absent in the spectrum of a monolayer (Fig. 1a). The antiparallel plasmonic dipoles are evidenced by the simulated electrical current distributions in the two layers (Fig. 1c). At the resonance frequency of the dark plasmon the currents in the two layers are strongly enhanced and have opposite direction. When increasing the film thickness by stacking more nanoparticle layers, additional dark plasmon modes form within the film and the plasmon frequencies shift.[10]

The carrier dynamics following the plasmon dephasing can be described by four separate steps: 1) the non-radiative damping channels result in a non-thermal distribution of excited carriers. 2) Electron-electron scattering leads to a bath of hot electrons in thermal equilibrium. 3) Electron-phonon coupling transfers the electron heat into phonons, which 4) dissipate the heat into the environment.[1,7,15,16] The strong increase in electron temperature after electron-electron scattering leads to a change in the gold dielectric function which results in a broadening of the plasmon resonance.[16,17] Monitoring this broadening after optical excitation via a pump-probe experiment gives direct access to the electron temperature. This way, the magnitude of the (thermalized) hot-electron generation depending on a specific excitation can be investigated in a transient absorption (TA) experiment.

III. RESULTS AND DISCUSSION

We prepared films of hexagonally close-packed AuNPs with different layer numbers. These were produced by self-assembly of colloidal AuNPs at a liquid-liquid interface and deposition on a quartz substrate. The exact synthesis technique was described elsewhere.[18] Analyzing transmis-

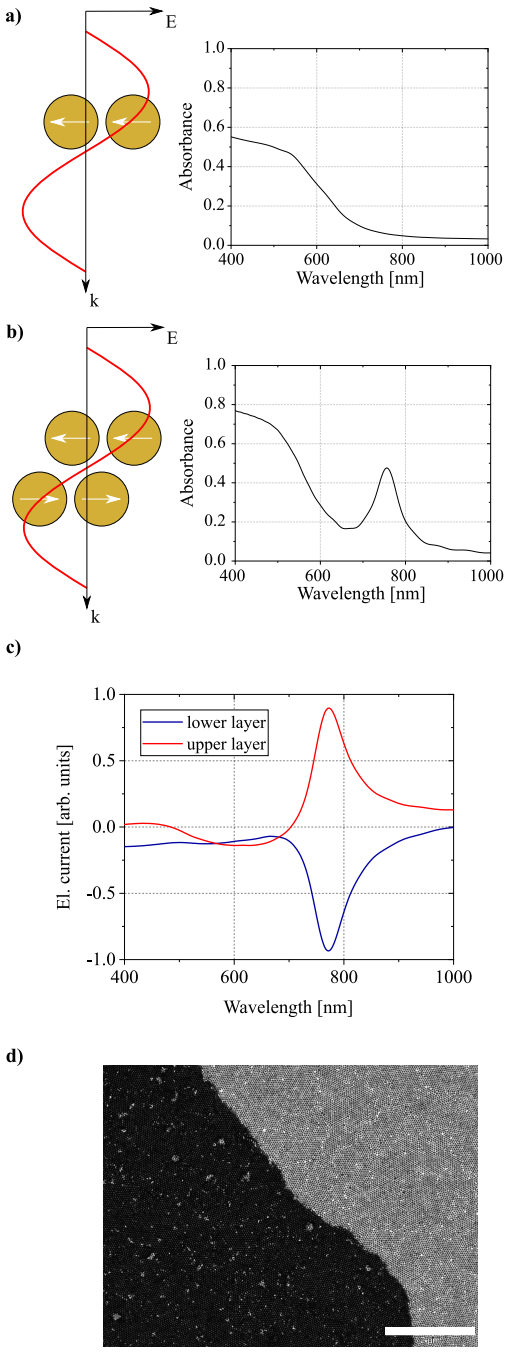

FIG. 1. Schematic plasmonic excitation in a monolayer (a) and a bilayer (b) of AuNPs with respective absorption spectra simulated by FDTD for hexagonally close-packed 42 nm AuNPs with a gap size of 3 nm. At normal incidence, the phase offset of the electric field between the two layers can excite antiparallel plasmonic dipoles. The additional peak around 750 nm is a dark plasmon excitation. (c) Magnitude of the electrical current in a bilayer of hexagonally close-packed AuNP. (d) TEM image of a mono- and bilayer of self assembled AuNPs of 42 nm diameter. The scale bar measures 2 µm. A higher resolution TEM image can be found in the SI.

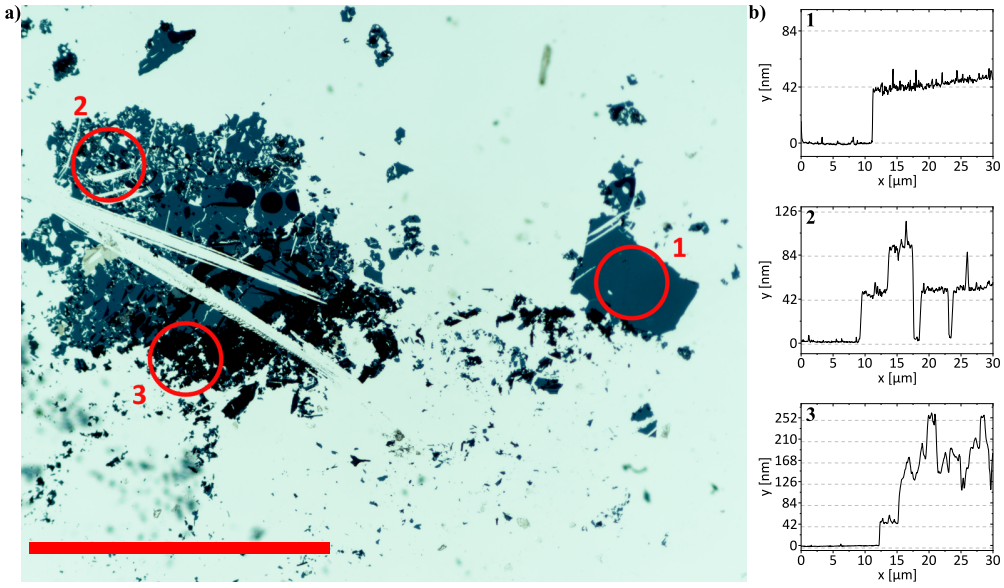

FIG. 2. Left: Optical microscopy image of the sample under investigation. The scale bar corresponds to 1 mm. The red circles indicate the spots measured in the TA experiments. Right: Exemplary AFM height profiles for the corresponding spots.

sion electron microscopy (TEM) images, one of which is shown in Fig 1d, the AuNP size was determined to be (42 ± 3) nm with an average interparticle gap size of approximately 4 nm. Optical microscopy allows distinguishing between mono-, bi- and multilayers (cf. Fig. 2a) as these lead to different saturation levels at a given illumination intensity. From the microscopy images, the relative coverage of the sample was determined at three distinguishable spots (see Tab. I). Exemplary height profiles obtained by atomic force microscopy (AFM) (see Fig. 2b) confirm, that spot 'mono' consists of a monolayer of AuNPs, while spots 'mixed' and 'multi' consist of increasing numbers of layers.

The microabsorbance spectra for specific layer numbers displayed in Fig. 3a show that in the near infrared wavelength region (700 nm to 1000 nm) new plasmon peaks occur with additional layers. These were identified as dark plasmon modes using finite-difference time-domain (FDTD) simulations shown in Fig. 3b: For two or more layers of AuNPs, dark plasmon modes lead to an increased absorption at excitation wavelengths between 700 nm and 1100 nm. The electrical currents obtained by the FDTD simulations within the layers at the corresponding plasmon energy, given in Fig. 1c, confirm the antiparallel orientation of the dipole moments in the layers. A similar analysis was conducted in our previous work for up to five layers.[10]

TABLE I. Coverage of the three spots measured in the TA experiment of the 42 nm AuNP superlattice. These values were obtained from a number of microscopy images with a larger magnification than the overview shown in Fig. 2a (for examples see Supporting Information).

spot	monolayer [%]	bilayer [%]	≥3 layers [%]
1 'mono'	100	0	0
2 'mixed'	67	23	10
3 'multi'	21	16	63

TA spectroscopy was employed to investigate the hot-electron generation via dark plasmon modes. The three representative spots marked in Fig. 2a were excited with wavelengths varying between 450 nm and 1050 nm. Because the increase of the electronic temperature leads to a change in the dielectric constant of the AuNPs, the plasmon resonance broadens upon excitation of hot electrons. We tracked the resulting transient bleach in the TA spectra (cf. Fig. 4a and additional spectra in the Supporting Information) at a fixed probe wavelength of 590 nm, which corresponds to the maximum bleach observed in the TA spectra. The wavelengths at which dark plasmons can be observed could not be probed, because a 750 nm-short pass filter was used to block the residual pump beam for the white light generation. To exclude probe-wavelength dependencies on the dynamics, we performed the same fit procedures described below at the positive TA signal around 500 nm. The results agreed well with the probe at 590 nm, suggesting that the TA spectrum decays homogeneously. The decay of the transient absorption signal shown in Fig. 4a is the result of the AuNP plasmon absorption narrowing due to the cooling of the hot carriers via electron-phonon (e-ph) coupling. We fitted the resulting decay curve using a two-exponential function (see Fig. 4b). The fast component of this decay is interpreted as the e-ph coupling time τ_{e-ph}.

Because the e-ph coupling strength in AuNPs is mostly constant, τ_{e-ph} is proportional to the initial temperature of the electron gas and a good indicator for the hot electron generation.[16] It has to be noted that the e-ph coupling times obtained in this experiment are very sensitive to the excitation power, which was held constant in all measurements. Usually, extrapolating the e-ph coupling times measured at varying excitation powers and fixed wavelengths leads to more robust results.[16,19,20] However, this technique could not be employed in this experiment due to a low signal to noise ratio for measurements on multilayers at low excitation power and sample degra-

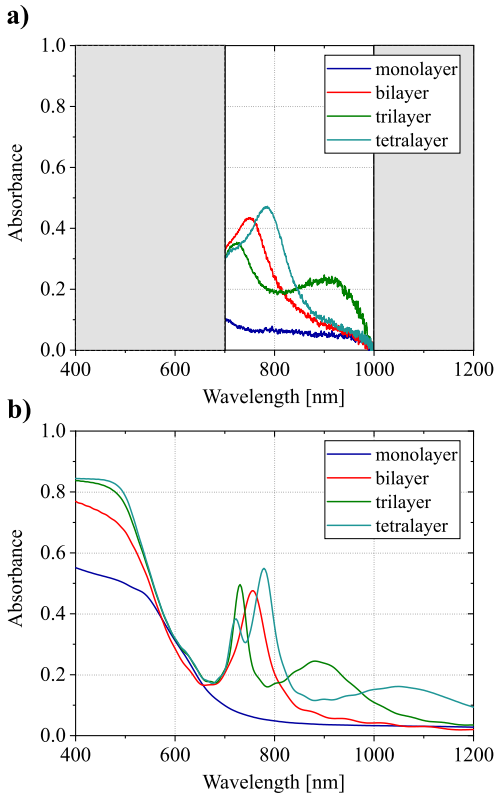

FIG. 3. a) Microabsorbance spectra of up to four layers of AuNP. The spectral range of this experiment was limited to the near infrared. b) FDTD simulations of the absorbance spectra of multiple layers of 42 nm AuNPs with a gap size of 3 nm.

dation at higher power. For calibration purposes, we analyzed a power series of a thicker, more robust sample (see appendix). There, the e-ph coupling time scales linearly with power and the linear regressions all start around (1.0 ± 0.1) ps.[11] Because of the linearity and uniform intercept, the observed differences for fixed powers and different excitation wavelengths are directly related to the different power-dependent slopes for the different wavelengths. We therefore assume the observed values for the e-ph coupling time in this study to result from different scaling with the excitation power.

The resulting τ_{e-ph} for the three spots indicated above are displayed in Fig. 4c. We observe the highest values at an excitation wavelength of 450 nm (2.37 ps, 2.27 ps and 3.11 ps, respectively). This large offset to the values at higher wavelengths results from interband transitions, which are excitable below a wavelength of approximately 520 nm.[17] At excitation wavelengths of 550 nm and 650 nm, where FDTD simulations in Fig. 3b show a similar absorbance for all three spots, the e-ph coupling times obtained in our experiments coincide. For the excitation wavelengths of

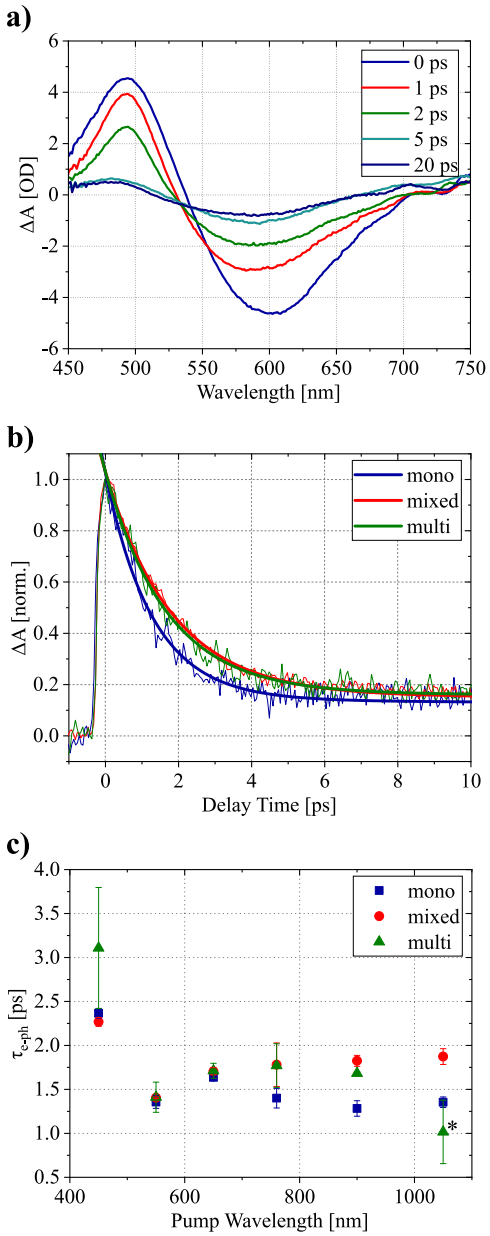

FIG. 4. a) TA spectra obtained with an increasing delay time for spot 'mixed' at an excitation wavelength of 900 nm. b) Normalized transient absorption signal (thin lines) and the respective fits (bold lines) for the spots indicated in Fig. 2a obtained at an excitation wavelength of 900 nm. c) Resulting electron-phonon coupling times τ_{e-ph} for the three spots for all excitation wavelengths. (*) This measurement could not be fitted well due to a low signal-to-noise ratio (see appendix).

760 nm, 900 nm and 1050 nm, which correspond to the resonance frequencies of dark plasmon modes in AuNP multilayers (cf. Fig. 3a), the e-ph coupling times for spots 'mixed' and 'multi' are increased by 0.37 ps to 0.54 ps compared to spot 'mono'.

In our earlier study we observed an increased e-ph coupling time when strongly absorbing interband transitions were excited in colloidal AuNPs as well. However, excitation around the bright plasmon mode did not lead to an observable increase in the e-ph coupling time although UV-Vis spectra show a clear absorption peak around that wavelength regime.[17] One can therefore assume that radiative damping results in less energy being dissipated into the electronic system.

Direct excitation of the dark plasmon modes leads to a significant increase in the e-ph coupling time. These results suggest that the increased absorption by dark plasmon modes indeed directly translates to an increased generation of hot carriers in AuNP multilayers. As explained in the theory section, non-radiative (Landau) damping is the prominent decay pathway for dark plasmons while radiative plasmon damping is suppressed. This effect benefits the excitation of hot charge carriers in that more light is absorbed by the particle and the initial electronic temperature after electron-electron scattering is increased. The increase in the initial electronic temperature leads to elevated e-ph coupling times in the TA experiment.

The results are contrary to the study of e-ph coupling in unordered films of colloidal AuNPs by Feldstein et al.[9], who found a decreasing e-ph coupling time with increasing film thickness. In disordered films of 12 nm AuNP, dark modes do not form in comparable ways. This underlines the importance of the film structure (hexagonal order vs. unordered) and particle size (42 nm vs. 12 nm) for exciting dark plasmon modes and subsequently for an increased generation of hot electrons with increasing layer number.

IV. CONCLUSION

Using transient absorption spectroscopy we have measured the e-ph coupling time in hexagonally close-packed AuNP mono- and multilayers. We found an increased e-ph coupling time at pump wavelengths corresponding to the excitation of dark plasmon modes. These results confirm that the excitation of dark plasmon modes in AuNP multilayers directly translates into hot electrons, which can be attributed to the vanishing net-dipole of dark plasmons and the corresponding suppression of their radiative decay leading to an enhanced absorption. While interband transitions, which are also an effective absorption channel for the generation of hot electrons, are not tunable, dark plasmon modes depend on AuNP size and arrangement. This enables improving the generation of hot carriers at a specific wavelength by adjusting the geometry of the material. In such a way dark plasmon modes are promising for studying light-matter coupling in plasmonic

materials as well as for developing more efficient materials for light-energy conversion.

V. METHODS

A. Transient absorption measurements

Transient absorption measurements were conducted using a commercial TA spectrometer (Helios, Ultrafast Systems). Seed pulses with a center wavelength of 800 nm and a pulse length of 35 fs were produced via chirped pulse amplification (Spitfire Ace, Spectra Physics) at a repetition rate of 1 kHz. Part of the beam seeded an optical parametric amplifier (TOPAS Prime/NIRUVis, Light Conversion) which allows adjusting the wavelength for the pump beam between 290 nm and 1600 nm. Every second pulse of this beam was blocked using a 500 Hz chopper in the TA spectrometer and the pump intensity was kept constant at 100 nJ/pulse (200 μJ/cm^2).

The second part of the seed beam passed a delay stage before being focused onto a 2 mm thick sapphire crystal to generate a white light continuum between 400 nm and 750 nm for the probe beam. The pump and probe beam overlapped in the sample in a non-collinear fashion to reduce the signal measured from the pump beam. The sample was fixed on a 3D translation stage to adjust the position of the beams on the sample.

Differential absorbance spectra were obtained by subtracting the spectrum of an unexcited sample from the spectrum of the excited sample. Three scans were performed for each setting and the average of these were used to further analyze the data. These data were corrected for chirp and scattered light in Surface Explorer (Ultrafast Systems).

To obtain the e-ph coupling time the transient signal at a probe wavelength of 590 nm was normalized to the local minimum of the bleach signal and fitted using a biexponential function given in Eq. 1. The time constant of the first exponential term τ_{e-ph} corresponds to the e-ph coupling time.

$$\Delta A = a * \exp\left(-\frac{t}{\tau_{e-ph}}\right) + b * \exp\left(-\frac{t}{\tau_{ph-ph}}\right) \tag{1}$$

B. Micro-Absorbance measurements

For details on the micro-absorbance measurements we refer to Ref. 10. The light of a supercontinuum laser (Fianium) was guided into an inverted microscope (Olympus) and focussed by a

100x objective with 0.9 NA onto the sample. To avoid damage of the sample, the laser power was kept below 100 µW. The sample position was controlled with a motorized xy translation stage. The transmitted light was collected by a second 100x objective with 0.8 NA and guided into a fibre-spectrometer (Avantes). As a reference for the transmittance T, we recorded the transmittance through the glass substrate. The reflected light was separated from the incoming light with a beam splitter (ThorLabs) and detected by the fibre-spectrometer. We used the reflected light from a silver mirror as reference for the reflectance R. The absorbance was calculated as $A = 1 - T - R$.

C. Finite-difference time-domain simulations

Finite-difference time-domain (FDTD) simulations were carried out with the commercial software Lumerical FDTD Solutions. For details we refer to Refs. 10 and 14. The gold nanoparticle layers were constructed by defining the unit cell of a single layer and using periodic boundary conditions along x and y. Gold nanospheres with diameter d were arranged in a hexagonal lattice and spaced apart by an interparticle gap size g. These layers were stacked along z into an hexagonally close-packed lattice of finite thickness. The optical properties of gold were modelled with a fit of the dielectric function measured by Johnson and Christy[21]. A broad-band plane wave source was used to illuminate the nanoparticle layers. The transmitted and reflected light was recorded with power monitors and the absorbance was calculated as $A = 1 - T - R$. The electical currents were calculated as the average of seven current monitors in each of the nanoparticle layers. The values were corrected for the wavelength-dependent phase shift that is accumulated when light propagates from the source to the nanoparticle layers.

ACKNOWLEDGMENTS

D.H., F.S. and H.L. wish to acknowledge the German Research Foundation (DFG) for their financial support via the Clusters of Excellence "Advanced Imaging of Matter" and "The Hamburg Centre for Ultrafast Imaging" (EXC 2056 – Project No. 390715994 and EXC 1074 – Project No. 194651731) and via the Project SCHU 3019/2-1. S.R. and N.S.M. were supported by the European Research Council under grant DarkSERS (772108).

REFERENCES

[1]G. V. Hartland, L. V. Besteiro, P. Johns, and A. O. Govorov, ACS Energy Letters **2**, 1641 (2017), https://doi.org/10.1021/acsenergylett.7b00333.

[2]J. Zhao, S. C. Nguyen, R. Ye, B. Ye, H. Weller, G. A. Somorjai, A. P. Alivisatos, and F. D. Toste, ACS Central Science **3**, 482 (2017), https://doi.org/10.1021/acscentsci.7b00122.

[3]C. Wang, X.-G. Nie, Y. Shi, Y. Zhou, J.-J. Xu, X.-H. Xia, and H.-Y. Chen, ACS Nano **11**, 5897 (2017), https://doi.org/10.1021/acsnano.7b01637.

[4]M. D. Brown, T. Suteewong, R. S. S. Kumar, V. DInnocenzo, A. Petrozza, M. M. Lee, U. Wiesner, and H. J. Snaith, Nano Letters **11**, 438 (2011), https://doi.org/10.1021/nl1031106.

[5]C. Clavero, Nature Photonics **8**, 95 (2014).

[6]S. V. Boriskina, T. A. Cooper, L. Zeng, G. Ni, J. K. Tong, Y. Tsurimaki, Y. Huang, L. Meroueh, G. Mahan, and G. Chen, Advances in Optics and Photonics **9**, 775 (2017).

[7]A. M. Brown, R. Sundararaman, P. Narang, W. A. Goddard, and H. A. Atwater, ACS Nano **10**, 957 (2016), http://dx.doi.org/10.1021/acsnano.5b06199.

[8]A. Brandstetter-Kunc, G. Weick, C. A. Downing, D. Weinmann, and R. A. Jalabert, Physical Review B **94**, 205432 (2016).

[9]M. J. Feldstein, C. D. Keating, Y.-H. Liau, M. J. Natan, and N. F. Scherer, Journal of the American Chemical Society **119**, 6638 (1997).

[10]N. S. Mueller, B. G. M. Vieira, F. Schulz, P. Kusch, V. Oddone, E. B. Barros, H. Lange, and S. Reich, ACS Photonics **5**, 3962 (2018), https://doi.org/10.1021/acsphotonics.8b00898.

[11]N. S. Mueller, B. G. M. Vieira, D. Höing, F. Schulz, E. B. Barros, H. Lange, and S. Reich, Faraday Discuss. (2018), 10.1039/C8FD00149A.

[12]S. K. Ghosh and T. Pal, Chemical Reviews **107**, 4797 (2007), pMID: 17999554, https://doi.org/10.1021/cr0680282.

[13]H. Lange, B. H. Juárez, A. Carl, M. Richter, N. G. Bastús, H. Weller, C. Thomsen, R. von Klitzing, and A. Knorr, Langmuir **28**, 8862 (2012), pMID: 22416809, https://doi.org/10.1021/la3001575.

[14]B. G. M. Vieira, N. S. Mueller, E. B. Barros, and S. Reich, The Journal of Physical Chemistry C **123**, 17951 (2019), https://doi.org/10.1021/acs.jpcc.9b03859.

[15]M. Bernardi, J. Mustafa, J. B. Neaton, and S. G. Louie, Nat. Commun. **6** (2015), 10.1038/ncomms8044.

[16]A. M. Brown, R. Sundararaman, P. Narang, A. M. Schwartzberg, W. A. Goddard, and H. A. Atwater, Phys. Rev. Lett. **118**, 087401 (2017).

[17]E. Minutella, F. Schulz, and H. Lange, The Journal of Physical Chemistry Letters **8**, 4925 (2017), https://doi.org/10.1021/acs.jpclett.7b02043.

[18]F. Schulz, S. Tober, and H. Lange, Langmuir **33**, 14437 (2017), https://doi.org/10.1021/acs.langmuir.7b03600.

[19]G. V. Hartland, Chemical Reviews **111**, 3858 (2011), http://dx.doi.org/10.1021/cr1002547.

[20]J. R. M. Saavedra, A. Asenjo-Garcia, and F. J. Garcia de Abajo, ACS Photonics **3**, 1637 (2016), http://dx.doi.org/10.1021/acsphotonics.6b00217.

[21]P. B. Johnson and R. W. Christy, Phys. Rev. B **6**, 4370 (1972).